J. Sustain. Metall. (2015) 1:151–160
DOI 10.1007/s40831-015-0009-5

RESEARCH ARTICLE

Extraction of Rare Earth Elements from Permanent Magnet Scraps by $FeO–B_2O_3$ Flux Treatment

Yuyang Bian · Shuqiang Guo · Lan Jiang · Kai Tang · Weizhong Ding

Published online: 30 January 2015

Abstract In order to recover the rare earth elements (REEs) from neodymium permanent magnet scraps, Fe_2O_3, B_2O_3, and $FeO–B_2O_3$ fluxes were designed to extract the REEs. The REEs containing oxides were successfully separated from the Fe-based metals at the temperatures of 1,673, 1,773, and 1,823 K. A mechanism for extraction of REEs has been proposed based mainly on the experimental observations using the flux of $FeO{\cdot}B_2O_3$ at 1,573 K. Effects of temperature and reaction time were also investigated. The experimental results have shown that increasing temperature and prolonging holding time help the reduction of B_2O_3 contents in the oxide phase. The $FeO–B_2O_3$ fluxes show better extraction efficiency. The purity of rare earth oxide was 98.4 % produced by $2FeO{\cdot}B_2O_3$ and the extraction ratios were higher than 99.5 % after the $FeO–B_2O_3$ fluxes treatment.

Keywords Rare earths · Permanent magnet · Extraction · Recycling

Introduction

The NdFeB permanent magnets contain more than 30 mass% of rare earth elements [1]. It is estimated that 20–30 % neodymium magnets scraps will be produced in the manufacturing process, e.g., processing, sintering, cutting, and polishing [2]. Furthermore, neodymium magnets are very easily oxidized at high working temperatures [3, 4]. The oxidized scraps cannot be reused in the conventional NdFeB magnet production chain. It is, thus, essential to recycle and extract the rare earth elements from magnet scraps [5, 6].

The conventional ways to extract rare earth elements from permanent magnet are mainly based on hydrometallurgical routes [7]. In these wet processes, huge amounts of water and chemicals, including industrial acids and alkalis, have to be used. These processes bring unavoidable environmental issues. On the other hand, the processes based on the high temperature pyrometallurgical treatments have now attracted more attention for their smaller environmental impacts. Owing to the strong affinity of oxygen to rare earth elements, Nakamoto et al. reported the extraction of REEs in the form of oxides from neodymium magnetic sludge in 2011 [1]. They found that the boron oxide concentration in the slag phase was decreasing with increasing the holding time in a graphite crucible at 1,723 K. The extraction of Nd from the waste NdFeB alloys by the glass slag method was also proposed by Saito et al. in 2003 [8]. Boron oxide was used as the extraction agent. In 2002, Uda used $FeCl_2$ to recover the rare earths from magnet sludge by transforming the REEs to corresponding rare earth chlorides, and further purifying the rare earth chlorides by vacuum distillation [9]. In 2006, Takeda et al. used magnesium as extraction medium to extract the REEs from the magnet scraps [10]. The rare earth elements were extracted from the magnets as Mg–Nd alloys, and REEs were further separated from the alloys by vacuum distillation of Mg from the Mg–Nd alloys. The use of silver as liquid metal extraction agent was also proposed. The rare earth oxides were the final products by this process [11]. Some other methods, known as slag extraction method [12],

Y. Bian · S. Guo (✉) · L. Jiang · W. Ding
Shanghai Key Laboratory of Modern Metallurgy and Materials Processing, Shanghai University, Shanghai 200072, China
e-mail: sqguo@shu.edu.cn

K. Tang
SINTEF Materials and Chemistry, 7465 Trondheim, Norway

electrolysis method [13], and carbonylation method [14], also provide alternative ways to recover the REEs from permanent magnets.

From the thermodynamic point of view, the fluxes of $FeO–B_2O_3$ are more favorable for the selective oxidation of neodymium in magnet scraps. In the present work, the optimized conditions for selective extraction of the REEs from the neodymium magnet scraps have been studied experimentally. Since the boron oxide was the major impurity in the rare earth oxides, the effects of experimental temperature and holding time on boron concentrations have been extensively studied. Influence of alumina on the rare earth oxides phase was also examined.

Materials and Method

Materials

Commercial neodymium magnets were used in the present work. The compositions of the magnets, determined by ICP-AES, are listed in Table 1. In order to accelerate the high temperature selective oxidation process, the commercial neodymium ingot was first pulverized mechanically to fine particles <75 μm. Ferrous oxalate dehydrate with purity >98 mass% and boric acid with purity >99.5 mass% were used to synthesize the fluxes of $3FeO·B_2O_3$, $2FeO·B_2O_3$ and $FeO·B_2O_3$. $FeC_2O_4·2H_2O$ and H_3BO_3 were first mixed with appropriate molar ratio. The mixture was preheated in an iron crucible at 673 K for 5 h under Ar atmosphere for decomposing the oxalate and eliminating the moisture. Then, the mixture was melted at about 100 K higher than the liquidus temperature for 2 h and cooled down to room temperature under inert atmosphere [15]. Iron oxide with purity >99 mass% and boron oxide with purity >98 mass% were also used as oxidizing agent in the present study.

Characterization

All the samples were examined with optical microscopy. The micro-structure of the samples and the distributions of the REEs were measured with backscattered-electron (BSEM) and energy dispersive spectrometry (EDS) detectors. The rare earth oxides were also characterized by X-ray diffraction (XRD) with Cu–Kα radiation. The contents of Nd, Pr, La, Al, Fe, and B in oxide phases were determined by inductively coupled plasma atomic emission spectrometry (ICP-AES) and the carbon contents were measured by Leco CS-600.

Table 1 Composition of the magnet ingot (mass%)

Fe	Nd	Pr	La	B	Al
61.60	30.73	4.39	1.58	0.96	0.83

Experimental Procedures

An electric furnace with $MoSi_2$ heating elements was used in the present experiments. The temperature was measured by a Pt–Rh(30 %)/Pt–Rh(6 %) thermocouple. Details of the experimental setup are given in Fig. 1. For protecting the graphite crucible and accelerating diffusion of carbon in selective oxidation process, pure graphite powder was put on the bottom of the crucible (32 mm inner diameter and 50 mm height). The neodymium magnet powders were then placed into the crucible. The oxidizing agent was placed on the top of neodymium magnet particles. The samples were heated up to the 1,573, 1,673, 1,773, or 1,823 K, and then held for 1, 4, or 9 h in a fixed Ar gas flow (200 ml/min). After the reaction, the sample was cooled down to room temperature in the furnace.

Results and Discussion

Preparation of $FeO–B_2O_3$ Fluxes and Thermodynamic Considerations

The $FeO–B_2O_3$ fluxes of $3FeO·B_2O_3$, $2FeO·B_2O_3$ and $FeO·B_2O_3$ with fixed mole ratio of FeO/B_2O_3 at 3, 2, and 1, respectively, were prepared by $FeC_2O_4·2H_2O$ and H_3BO_3. The crystal structure of the fluxes at room temperature after high temperature treatment is shown in Fig. 2. Only the binary compound, $Fe(BO_2)_2$, exists in the fluxes. With the increase of FeO in the fluxes, the patterns of $Fe(BO_2)_2$ were enhanced. Moreover, the diffraction patterns of B_2O_3 and Fe_3O_4 were also detected in the diagram.

Considering the volatilization of boron oxides during the fluxes preparation, the concentration of Fe and B were measured after the preparation of the fluxes, and are listed in Table 2. The concentrations of Fe and B in the fluxes are close to the theoretical values. It is concluded that the volatilization of boron oxides did not occur significantly during the preparation of the fluxes. This is attributed to the formation of $Fe(BO_2)_2$ that stabilizes boron oxides, especially in the fluxes with high iron concentration. The prepared $FeO–B_2O_3$ fluxes also with B_2O_3 and Fe_2O_3 were used in the extractive experiments as oxidizing agents.

For the oxidative extraction of REEs from magnet scraps, the following reactions should be taken into considerations:

$$4/3Nd + O_2(g) = 2/3Nd_2O_3, \quad (1)$$

$$4/3Al + O_2(g) = 2/3Al_2O_3, \quad (2)$$

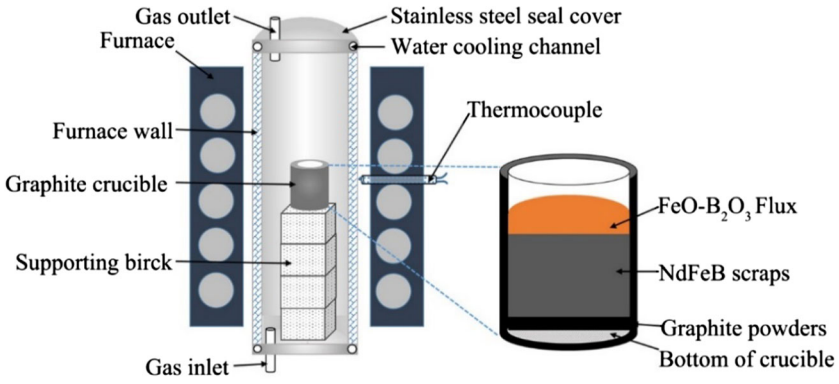

Fig. 1 Schematic diagram of apparatus used for the extraction experiments, and the illustration of the setup of the sample in graphite crucible

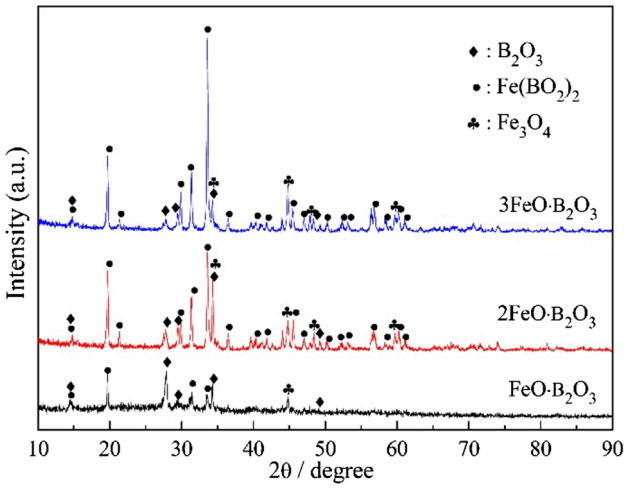

Fig. 2 The XRD patterns of the prepared fluxes of $3FeO{\cdot}B_2O_3$, $2FeO{\cdot}B_2O_3$, and $FeO{\cdot}B_2O_3$

Table 2 Theoretical and measured concentrations of Fe and B in the prepared fluxes

Fluxes	Theoretical (mass%)		ICP analyses (mass%)	
	Fe	B	Fe	B
$FeO{\cdot}B_2O_3$	39.5	15.3	35.80	15.29
$2FeO{\cdot}B_2O_3$	51.6	10.0	48.17	11.83
$3FeO{\cdot}B_2O_3$	57.5	7.4	55.21	8.19

$$4/3B + O_2(g) = 2/3B_2O_3, \quad (3)$$

$$4/3Fe + O_2(g) = 2/3Fe_2O_3, \quad (4)$$

$$2Fe + O_2(g) = 2FeO, \quad (5)$$

$$3/2Fe + O_2(g) = 1/2Fe_3O_4, \quad (6)$$

$$2C + O_2(g) = 2CO(g), \quad (7)$$

$$1/2Fe + B + O_2(g) = 1/2Fe(BO_2)_2. \quad (8)$$

Figure 3 shows the standard Gibbs free energy for the above reactions (1)–(8). The thermodynamic calculations were performed using HSC chemistry 5.1 software for Windows. The free energies of Pr_2O_3 and La_2O_3 are not presented in Fig. 3, because they are rather similar to Nd_2O_3 [16, 17], for example, the equilibrium constants of formation of Nd_2O_3, Pr_2O_3 and La_2O_3 at 1,823 K are 1.15×10^{37}, 1.10×10^{37}, and 3.91×10^{36}, respectively. The Ellingham diagram shows that the standard Gibbs free energy of formation of Nd_2O_3 is much more negative than those of Fe_2O_3, Fe_3O_4, FeO, B_2O_3, and $Fe(BO_2)_2$ and the reaction (1) is thermodynamically more feasible to occur than the others reactions.

Extraction of Rare Earth Elements from NdFeB Magnet

The NdFeB material consists of three phases: the $Nd_2Fe_{14}B$ matrix phase (T_1), the Nd-rich boundary phase, and $Nd_{1.1}Fe_4B_4$ phase (T_2) [18, 19]. The phase of $Nd_2Fe_{14}B$ was identified by the XRD analysis, as shown in Fig. 4. Because the contents of the other two phases were relatively smaller, the Nd-rich phase and $Nd_{1.1}Fe_4B_4$ phase overlapped in the XRD patterns. From the DSC curve of the NdFeB material, three peaks appeared, as marked in Fig. 5. Although the equilibrium phases were not characterized during the heating of DSC experiment, the peak (1), (2), and (3) can be expected to be reaction (9), (10), and (11), from the phase diagram evaluated by Hallemans et al. [19] and Van Ende and Jung [20]. In order to ensure the extraction process is going into liquid phase, the start temperature of Peak 3 is considered as the lowest experimental extraction temperature. In the following reactions (9)–(11), L, L′, and L″ represent different liquid phases during the melting process.

$$T_1 + T_2 + Nd = L'' + T_1 + T_2 \quad (9)$$

$$L'' + T_1 + T_2 = L' + T_1 \quad (10)$$

$$T_1 + L' = L + \gamma - Fe \quad (11)$$

In order to examine the separation efficiency of the oxide phase and the metal phase in the sample, an

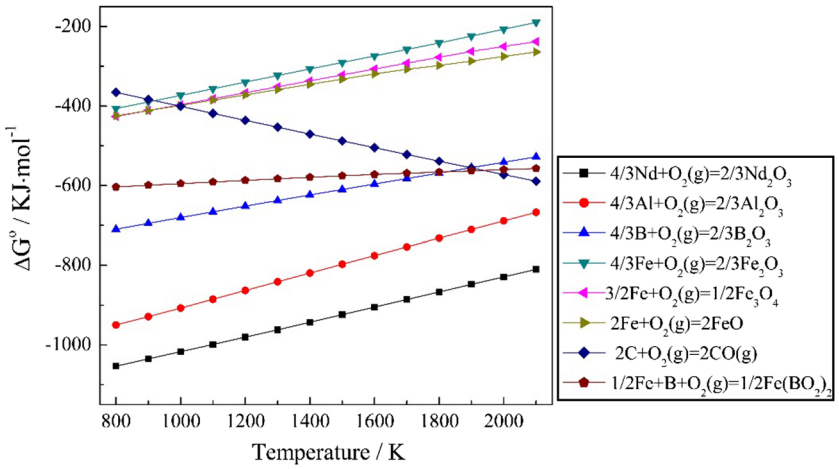

Fig. 3 Ellingham diagram of the species in the present study

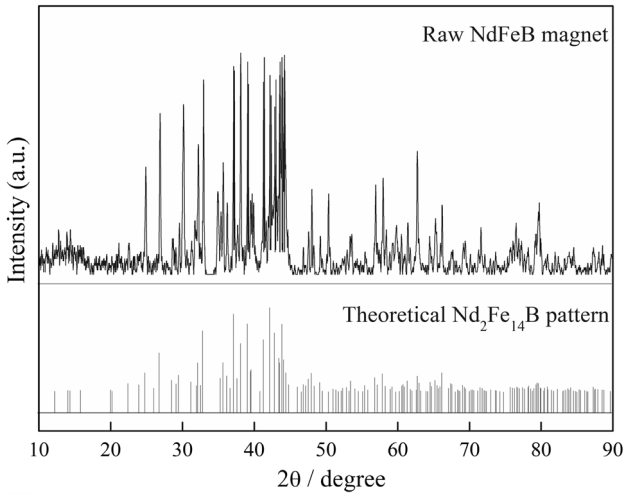

Fig. 4 XRD pattern of the raw experimental NdFeB magnet

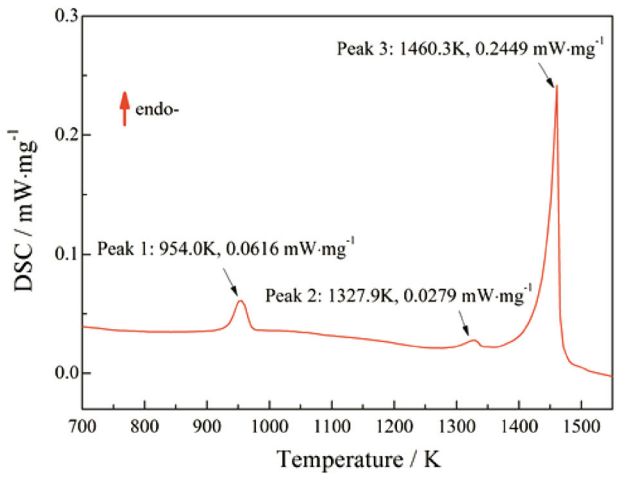

Fig. 5 The DSC curve of raw experimental magnet in Ar atmosphere (heating rate 10 K/min)

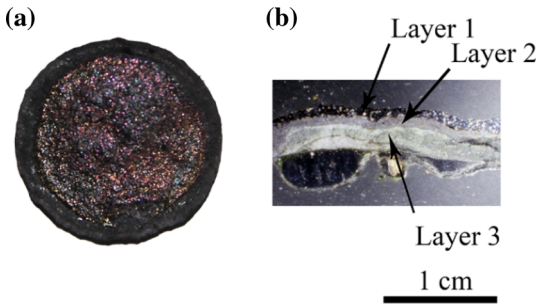

Fig. 6 Optical microscope image of the final sample obtained at 1,573 K for 9 h (**a**), and the cross-sectional morphology (**b**)

experiment was first carried out at 1,573 K for 9 h using the flux of $FeO{\cdot}B_2O_3$ as oxidizing agent. Figure 6(a) shows optical microscope images of the sample. In Fig. 6(b) three layers above the metal bath were observed. Layer 1 is a metal phase whereas layer 2 and 3 are the oxide phases. After separating these three different phases mechanically, they were characterized by XRD. The XRD patterns, as shown in Fig. 7, indicated that layer 1 was a metal phase containing mainly the α-Fe metal phase. Layer 2 was the rare earth borate, $REBO_3$. Layer 3 was the relative pure rare earth hydroxide, $RE(OH)_3$, probably hydrolyzed from the pure rare earth oxide [21]. Because the lattice constants of $NdBO_3$ and $PrBO_3$ are extremely close, they were not marked separately. The same treatment was also used to $RE(OH)_3$ and $REAlO_3$ in the following XRD identifications.

The above experimental results may help us to reveal the reaction mechanism of REEs' high temperature extraction process. The melting temperature of $FeO{\cdot}B_2O_3$ and of $Nd_2Fe_{14}B$ are about 1,090 K [15] and 1,400 K (as shown in Fig. 5), respectively. Both the magnet scraps and flux were initially in the liquid states at 1,573 K under the

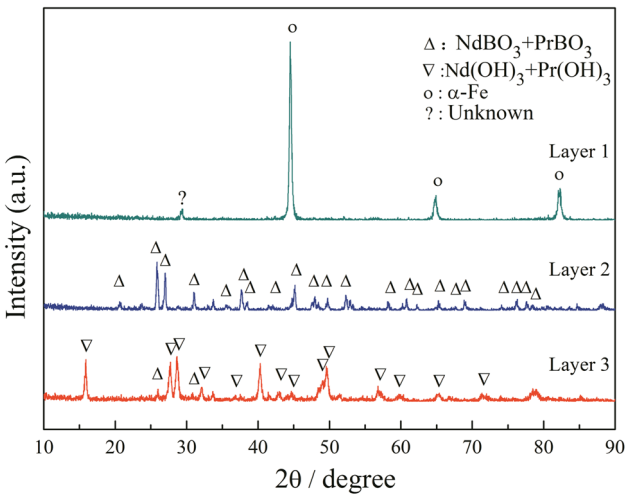

Fig. 7 The XRD patterns of different layers corresponding to Fig. 6(**b**)

present experimental conditions, as illustrated in Fig. 8(a). As mentioned before, FeO in molten flux possesses larger chemical potential to react with neodymium than B_2O_3. Initially, FeO in the flux is reduced by REEs in the metal bath, and the iron precipitated on the top of the sample. When interpreting the phenomenon of iron precipitation, it should be kept in mind that the difference of densities between the rare earth oxides (7.24 g/cm^3) and iron (7.86 g/cm^3) are rather small. The carbon content in the layer 1 metal phase was measured with the carbon analyzer, being around 0.07 mass%. It indicates that the iron layer was in solid form at 1,573 K, and no reduction of iron oxide by graphite in the crucible happened. This observation can also be confirmed by Fig. 6(a) from the differences of the diameters of iron layer and the oxide layer. After this process, the FeO was exhausted and RE_2O_3 was formed, which participated into the flux, forming the RE_2O_3–B_2O_3 fluxes, also illustrated in Fig. 8(b). The rare earth oxides and the boron oxides formed the rare earth borate, $REBO_3$. Reductions of B_2O_3 and $REBO_3$ by the remaining REEs in the metal bath then took place after most of FeO had been consumed, as illustrated by Fig. 8(c), and the RE_2O_3 layer formed.

Both the $REBO_3$ and RE_2O_3 are the high melting temperature compounds, with the melting point being about 1,850 K [22] and 2,590 K, respectively. The formations of these two solid layers will prevent further extraction of the REEs remaining in the metal bath. In order to accelerate the diffusion of boron in $NdBO_3$ and Nd_2O_3 and promote the extraction process, further increase of the experimental temperature is necessary.

Pictures of samples after the extraction processes are shown in Fig. 9. Figure 9(a–c) are the samples obtained at 1,673, 1,773, and 1,823 K for 9 h, respectively. Their cross-sectional pictures are shown in Fig. 9(d–f). Different from the sample obtained at 1,573 K, in all samples shown in Fig. 9, the Fe-rich metals and rare-earth-containing oxides were separated successfully. Most of the Fe remained in the metal phase. From the cross-sectional morphology, it can be seen that the oxide phases covered more evidently the metal phase, whereas the interface between the two phases became rough, as the experimental temperature increased [1].

Smaller metal droplets ranging from several millimeters to several microns, were also observed in the oxide phase. In order to separate the metal droplets from the oxide phase, magnetic separation was applied. Figure 10 shows the final separation for the sample carried out at 1,673 K for 9 h.

Rare Earth Elements in the Oxide Phase

In the experimental temperature range from 1,673 to 1,823 K, almost all REEs and Al in magnet scraps were extracted to the oxide phase. FeO, initially in the oxidizing agent, was reduced to the metal phase completely. The flux is in fact exceeding the value calculated by just fully oxidizing the rare earth elements in the magnet scraps, where normally the oxygen stoichiometric ratio is controlled at 1.3. Boron oxide that remained in the oxide phase could hardly be reduced completely by carbon. Under strongly

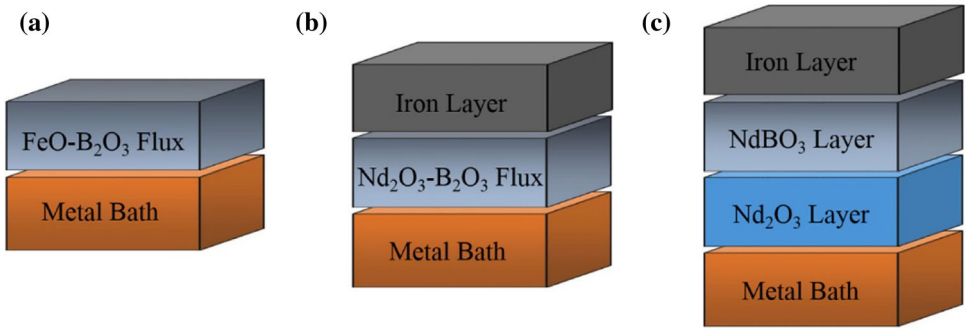

Fig. 8 The schematic diagram of the reaction mechanism of the REEs extraction process at 1,573 K

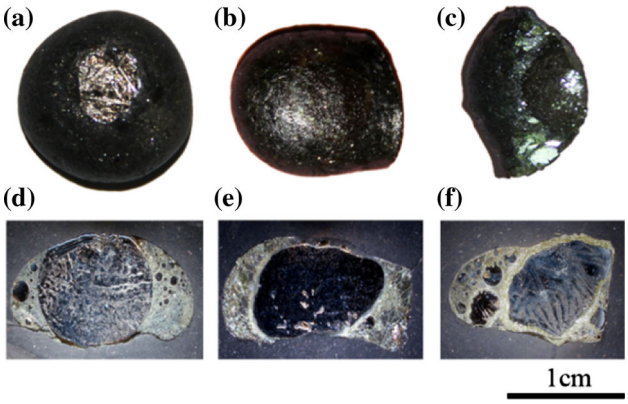

Fig. 9 Optical microscope image of the final sample obtained at **a** 1,673 K, **b** 1,773 K, **c** 1,823 K for 9 h, and the images **d**, **e**, and **f** are the cross section of (**a**), (**b**), and (**c**), respectively

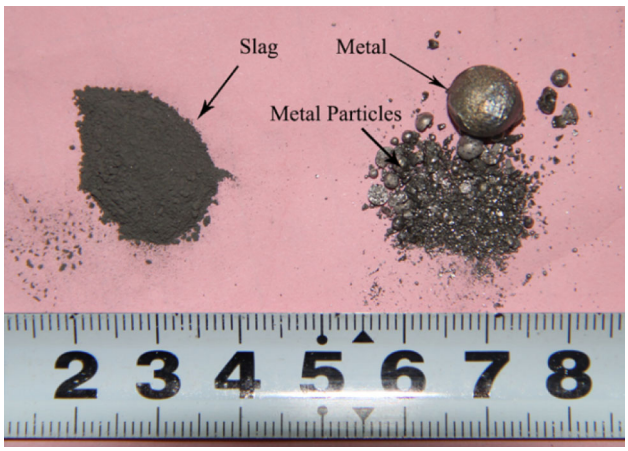

Fig. 10 Slag and metal after separation for the experiment at 1,673 K after 9 h

reducing conditions and in the experimental temperature range, any iron in the fluxes goes almost entirely into the metal phase. Neodymium, praseodymium, lanthanum, and aluminum always exist in the form of oxides. Only boron was distributed in both oxide and metal phase. Table 3 lists the chemical analysis results of the samples obtained in the present investigation. The concentrations of oxides were normalized.

For all experiments in the present study, as shown in Table 3, almost all earth elements have been extracted to the oxide phase. The extraction ratios of all REEs are more than 99 mass%, as defined by Eq. (a). Main impurities in the oxides are alumina and boron trioxide. The purity of the rare earth oxides is higher than 96 mass%, according to Eq. (b).

$$\text{Ratio of Extraction} = 1 - \frac{\text{Mass of REE in metal phase}}{\text{Mass of REE in raw NdFeB magnet}} \times 100\ \%, \quad \text{(a)}$$

$$\text{Purity} = \frac{\text{Mass of REO in oxide phase}}{\text{Mass of the oxide phase}} \times 100\ \%. \quad \text{(b)}$$

Both the sum of rare earth oxides and individual Nd_2O_3, Pr_2O_3, La_2O_3 contents are little dependent upon experimental temperature (1,673–1,823 K) and reaction time (1–9 h). This clearly indicates that the driving force for the heterogeneous reactions between metal and oxide phase is sufficiently high. Basically, boron oxide in fluxes can also be reduced to the metal phase by neodymium in the magnets. Reduction of iron oxide by rare earth elements is prior to the reduction of boron oxide in the fluxes, as proved both theoretically (Fig. 3) and experimentally (Figs. 6, 7). Under the experimental condition (1,673–1,823 K, 1–9 h) and the amount of extraction agents employed, all the rare earth in the metal phase were exhausted, and reduction of B_2O_3 in oxide phase was carried out by carbon from the metal phase [1]. Carbothermic reduction of B_2O_3 occurs at relatively high temperature, higher than 1,873 K, as shown in Fig. 3, with much weaker thermodynamic driving force. However, some researchers have investigated the production of boron carbides. The reaction becomes thermodynamically feasible above 1,673 K [23]. Chemical kinetics in this stage play an important role. Further reduction of B_2O_3 in oxide phase is a time-dependent process, as shown in Table 3. Of course, the process is also dependent

Table 3 Concentrations of the oxides and metals in different experimental conditions using the flux of $FeO{\cdot}B_2O_3$

Temperature (K)	Holding Time (h)	Oxide Phase (mass%)					Metal phase (mass%)					
		Nd_2O_3	Pr_2O_3	La_2O_3	Al_2O_3	B_2O_3	Nd	Pr	La	Al	B	C
1,823	1	79.63	11.45	5.25	1.76	1.92	0.10	0.01	<0.01	0.02	2.28	3.29
1,823	4	80.03	11.32	5.22	1.98	1.46	0.15	0.02	<0.01	0.03	2.82	3.52
1,823	9	81.55	11.24	4.87	1.82	0.51	0.13	0.02	<0.01	0.07	3.01	1.50
1,773	9	81.13	11.45	4.87	1.61	0.93	0.27	0.03	0.01	0.03	2.89	1.37
1,673	9	80.08	11.23	5.09	1.89	1.71	0.23	0.03	0.01	0.02	2.54	1.16

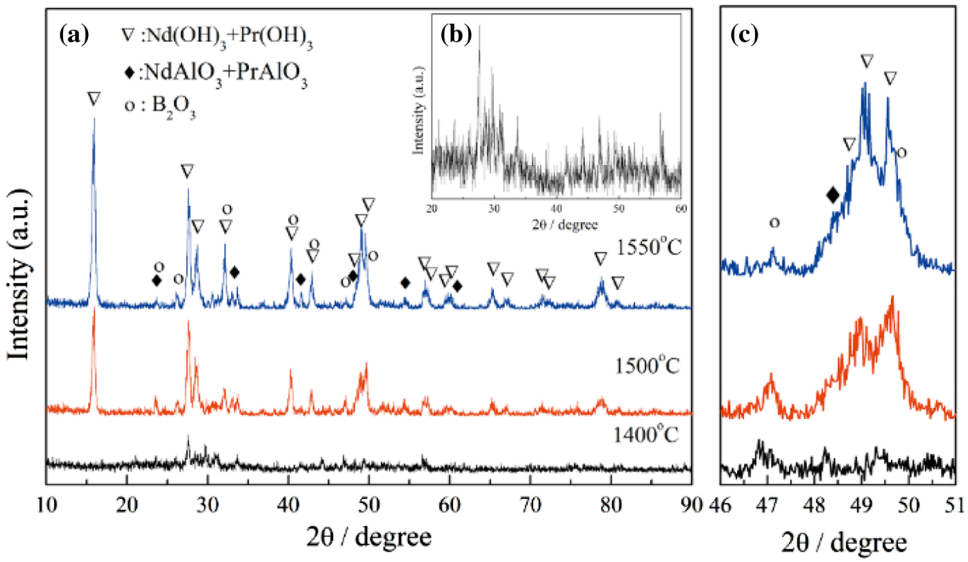

Fig. 11 XRD patterns of the oxides treated at different temperatures for 9 h **a** XRD patterns at 1,673, 1,773, and 1,823 K, **b** XRD pattern at 1,673 K from 20° to 60°, **c** partial enlargement of **a** from 46° to 51°

strongly upon temperature, since increasing temperature leads to an increase of the driving force of the reaction.

Rare earth oxides can easily absorb the moisture from air and form the hydroxides [21]. Almost all the rare earth oxides have converted to hydroxides after they were placed in air atmosphere for 72 h. Figure 11 shows the XRD analysis for the slag of the samples, displayed in Fig. 9. It is evidenced that the rare earth hydroxides are the main phases. The XRD patterns of $RE(OH)_3$ become stronger with less B_2O_3 content, as shown in Fig. 11(a). More boron oxides in the oxide phase will decrease the crystallinity of rare earth oxide phase and will improve the formation of the glass phase, as shown in Fig. 11(b). A perovskite phase of $REAlO_3$ also existed in the oxide phase, as shown in Fig. 11(a). It indicates that alumina in the oxide phase reacts with RE_2O_3 and finally forms the stable perovskite phase [24].

It is well known that the rare earth oxides and Al_2O_3 are chemically more stable than B_2O_3 and FeO. During the fluxing treatments, aluminum will be inevitably oxidized. Figure 12(a) shows a BSEM image of the oxide phase, where three main phases were observed: the dark phase in regular morphology, the gray phase in a needle-like form, and the basic white phase. The EDS pattern of BSEM image is shown in Fig. 12(b). It is observed that the peak of Al in the dark phase is higher than the white phase, and no Al was detected in the gray phase. Before the observation by BSEM, the sample was coated with Au to improve the electrical conductivity of the oxides, the peak of Au is also observed in Fig. 12(b). The quantitative analysis results of the EDS were normalized without regarding Au.

The EDS quantitative analyses are listed in Table 4. It shows that the atomic amount of Al is almost equal to the

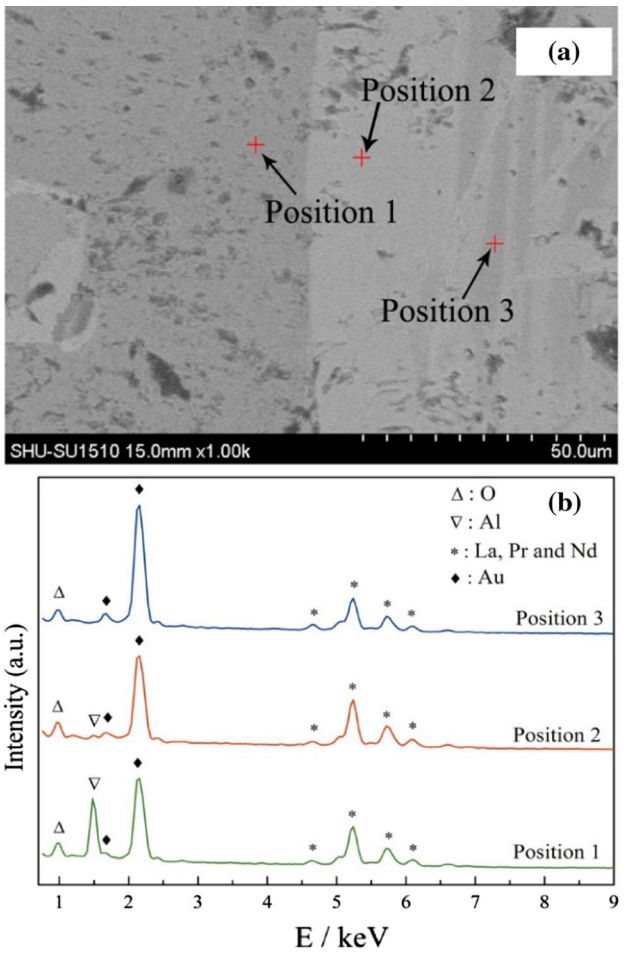

Fig. 12 The BSEM of the oxide phase (**a**), and the EDS patterns (**b**) to different positions of (**a**), and the analyzed chemical compositions are tabulated in Table 4

Table 4 Contents of different phases in the oxides determined by EDS corresponding to Fig. 12

	Dark phase		White phase		Gray phase	
	Mass%	Atom%	Mass%	Atom%	Mass%	Atom%
Nd L	62.63	25.78	75.86	41.45	73.07	50.53
Pr L	10.51	4.43	10.93	6.11	13.69	9.69
La L	2.86	1.22	2.52	1.43	7.75	5.56
Al K	13.54	29.79	0.81	2.35	*	*
O K	10.45	38.78	9.88	48.66	5.49	34.22

* Undetected

Table 5 Concentrations of the oxides and metals treated by different fluxes at 1,773 K

Exp. NO.	Oxidizing agent	Holding time (h)	Oxide phase (mass%)					Metal phase (mass%)					
			Nd_2O_3	Pr_2O_3	La_2O_3	Al_2O_3	B_2O_3	Nd	Pr	La	Al	B	C
1	Fe_2O_3	1	80.95	11.46	5.21	1.72	0.67	0.43	0.05	0.03	0.05	0.27	4.01
2	Fe_2O_3	4	81.03	11.18	5.04	2.03	0.72	0.77	0.01	<0.01	0.01	0.38	4.34
3	Fe_2O_3	9	81.73	11.39	4.97	1.35	0.56	0.79	0.10	0.06	0.14	0.54	3.35
4	$3FeO{\cdot}B_2O_3$	1	78.94	11.25	5.41	1.47	2.93	0.11	0.01	0.01	0.01	1.95	1.36
5	$3FeO{\cdot}B_2O_3$	4	80.07	11.39	5.40	1.57	1.57	0.03	<0.01	<0.01	0.01	1.50	2.98
6	$3FeO{\cdot}B_2O_3$	9	82.19	11.40	4.79	1.15	0.47	0.04	<0.01	<0.01	0.01	1.62	3.21
7	$2FeO{\cdot}B_2O_3$	1	79.50	11.18	5.32	1.32	2.68	0.06	0.01	<0.01	0.01	1.92	2.94
8	$2FeO{\cdot}B_2O_3$	4	81.47	11.50	5.30	1.14	0.59	0.02	<0.01	<0.01	0.01	2.71	2.60
9	$2FeO{\cdot}B_2O_3$	9	81.32	11.83	5.26	1.33	0.27	0.06	0.01	<0.01	0.02	2.35	2.76
10	$FeO{\cdot}B_2O_3$	1	78.71	11.62	5.14	1.32	3.21	0.08	0.01	0.01	0.02	2.49	2.77
11	$FeO{\cdot}B_2O_3$	4	81.23	11.90	5.00	1.14	0.73	0.04	0.01	<0.01	0.02	3.10	0.35
12	$FeO{\cdot}B_2O_3$	9	81.00	11.84	4.86	1.21	1.09	0.02	0.00	<0.01	0.01	2.97	2.51
13	B_2O_3	1	78.98	11.43	5.45	1.34	2.80	0.05	0.01	<0.01	0.05	4.00	2.03
14	B_2O_3	4	76.61	10.79	4.93	1.35	6.32	0.13	0.02	0.01	0.02	3.68	1.95
15	B_2O_3	9	80.26	11.58	5.61	1.56	0.98	0.05	<0.01	<0.01	0.03	4.26	1.78

atomic amount of RE (RE: Nd, Pr, and La) elements in the dark phase. It proves that the dark phase is the perovskite $REAlO_3$ phase, which has also been identified by the XRD patterns in Fig. 11. The gray phase is RE_2O_3 phase without alumina, and the white phase is RE_2O_3 containing a small percentage of alumina. Because the physicochemical properties of the RE_2O_3–Al_2O_3–B_2O_3 system are not well defined, the Al_2O_3 distribution in the oxide phase needs to be further studied.

Effects of Fe_2O_3, FeO–B_2O_3 Fluxes and B_2O_3 on the REEs Extraction

The effect of different oxidizing agents on the REEs extraction was further investigated using the fluxes of Fe_2O_3, $3FeO{\cdot}B_2O_3$, $2FeO{\cdot}B_2O_3$, $FeO{\cdot}B_2O_3$, and B_2O_3 for different times (1, 4, or 9 h) at 1,773 K. The concentrations of the oxide phase and the metal phase are listed in Table 5. The amount of flux exceeded the stoichiometric ratio of oxygen, and the ratio of all the experiments in Table 5 were fixed at 1.3.

Under these experimental conditions, the extraction ratios and the purities of rare earth oxides were calculated referring to Eq. (a) and Eq. (b), and shown in Fig. 13. The purities of rare earth oxides produced by the FeO–B_2O_3 fluxes and Fe_2O_3 improved apparently with the increase of reaction time, as shown in Fig. 13(a). However, the purities of rare earth oxides extracted by B_2O_3 fluctuated seriously, and the purities of these samples were rather lower. The extraction ratios by the extraction agents of FeO–B_2O_3 and B_2O_3 were similar. However, the extraction ratios by the oxidizing agents of Fe_2O_3 were relatively low. Based on the results in Fig. 13 and Table 5, it can be concluded that the FeO–B_2O_3 flux works better than pure Fe_2O_3 and B_2O_3. The extraction ratios and the purities of rare earth oxides are similar to the fluxes of FeO–B_2O_3. The highest purity of REO is 98.4 mass% when using the flux of $2FeO$–B_2O_3. The extraction ratios are higher than 99.5 % when using the fluxes of $3FeO{\cdot}B_2O_3$, $2FeO{\cdot}B_2O_3$, and $FeO{\cdot}B_2O_3$. This means that because the reaction Gibbs free energy for the formation of rare earth oxide by reduction of FeO is very negative, the difference of FeO activity in the FeO–B_2O_3

flux is hardly changing the driving force of the chemical reaction.

The dependency of B_2O_3 concentration in the oxide phase upon the reaction time is obviously for the fluxes of FeO–B_2O_3, as shown in Fig. 14(a). However, no clear tendency was obtained for the pure Fe_2O_3 or B_2O_3. The content of B_2O_3 in the oxide phase using Fe_2O_3 as oxidizing agent is relatively lower by holding for 1 h, but it hardly changed with an increasing holding time, whereas the content of remaining rare earth elements in the metal phase was the highest compared to the rare earth content in the metal phase, when using other oxidizing agents. This may be attributed to the fact higher levels of B_2O_3 help reduce the viscosity of the oxide phase [22]. As known, the rare earth oxides have a high melting point around 2,590 K. An adequate fluidity of the oxide phase improves the mass transfer of B_2O_3 in the oxides, and help to extract the remaining rare earth elements from the metal phase after the FeO has been consumed. The fluidity of the oxides was enhanced by adding B_2O_3. The remaining rare earth in the metal phase decreased dramatically. However, using B_2O_3 solely as oxidizing agent, when the equilibrium of Nd and Nd_2O_3 is reached, the remaining B_2O_3 will be reduced by carbon. And the driving force of reduction of B_2O_3 by carbon in the current experimental conditions is not sufficient.

Increasing B_2O_3 content in the fluxes resulted in a higher boron concentration in the metal phase. The interstitial solid solution of boron in the Fe matrix will decrease the content of carbon in the metal phase [25], as is clearly shown in the Fig. 14(b). The surface tension of the metal phase increases with a decreasing content of carbon and increasing content of boron in the iron matrix phase [26]. The surface tension of the metal melts produced by the oxidizing agents will increase with the increase of B_2O_3 in the fluxes. The difference of the densities of a high REO-containing oxide phase and the metal phase is small, hence, the surface free energy becomes an important factor in the separation of the oxide phase and the metal phase. Boron concentrating in the metal phase helps the separation of oxide phase and the metal phase. However, the increase of boron in metal phase will bring the reducing ability of carbon to B_2O_3 in the oxide phase down.

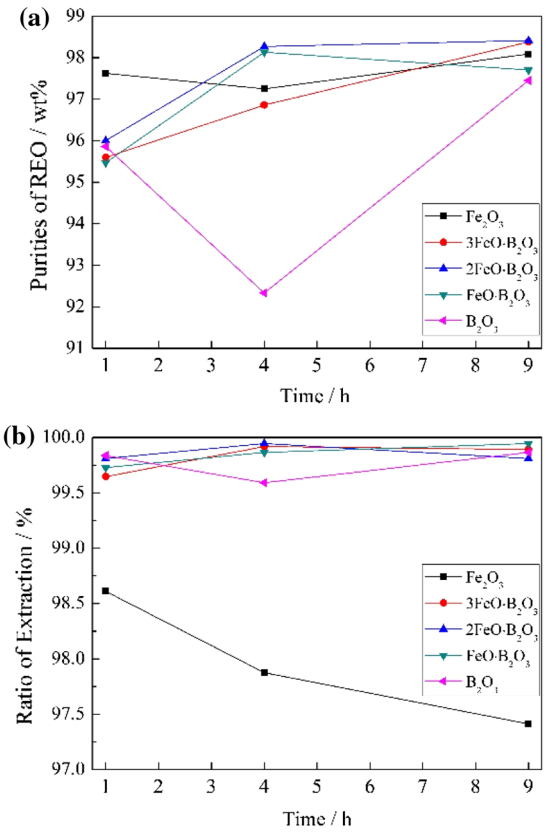

Fig. 13 The purities of REO (**a**), and the extraction ratios (**b**) by different fluxes at 1,773 K holding for 1, 4 and 9 h

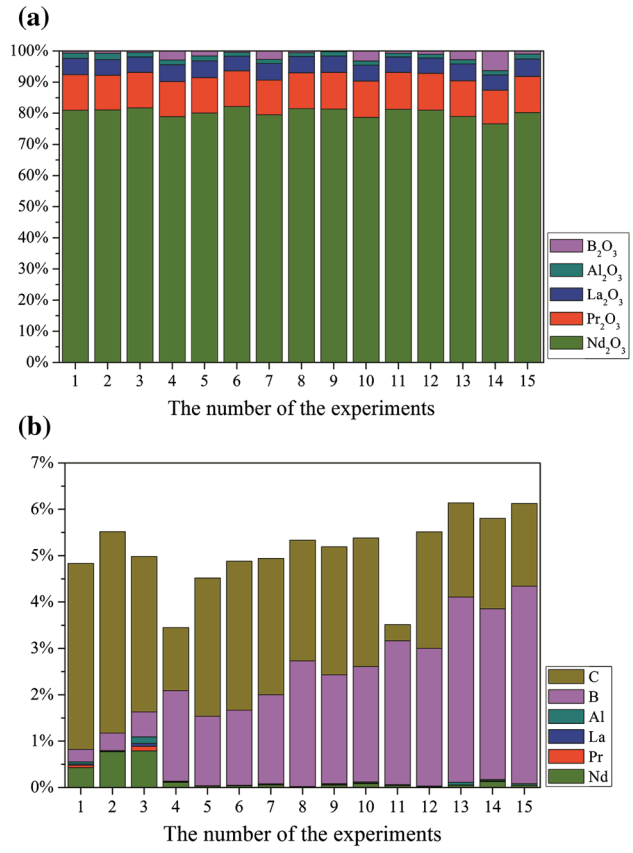

Fig. 14 Chemical concentration of oxides (**a**) and metals (**b**) treated by different fluxes at 1,773 K, and the corresponding experimental condition for given experimental number is tabulated in Table 5

Conclusions

Extraction of rare earth elements from magnet scraps by a range of $FeO–B_2O_3$ fluxes has been investigated in the present work. The reaction sequences for the samples at 1,573 K have been proposed as follows: FeO in the fluxes is firstly reduced by the rare earth elements, the initial formed rare earth oxides then react with B_2O_3 in the flux and form $REBO_3$. The $REBO_3$ is further reduced partially by the remaining rare earth elements and/or carbon in the metal bath. Increasing temperature and the experimental holding time help to reduce the boron oxides in the rare-earth-containing oxides.

The optimized composition of the fluxes has also been determined experimentally. Considering the purities of REO and the extraction efficiency, the $FeO–B_2O_3$ fluxes are better than pure Fe_2O_3 and B_2O_3. The highest purity of the rare earth oxides obtained from the present study can reach 98.4 mass% by the extraction agent of $2FeO{\cdot}B_2O_3$ and the extraction ratios for the rare earth elements are more than 99.5 mass% after the $FeO–B_2O_3$ treatments.

Acknowledgments This study was financially supported by the National Key Basic Research Program of China (973) (2012CB722805).

References

1. Nakamoto M, Kubo K, Katayama Y, Tanaka T, Yamamoto T (2011) Extraction of rare earth elements as oxides from a neodymium magnetic sludge. Met Mater Trans B 43:468–476
2. Itoh M, Miura K, Machida K-I (2009) Novel rare earth recovery process on NdFeB magnet scraps by selective chlorination using NH_4Cl. J Alloy Compd 477:484–487
3. Edgley DS, Le Breton JM, Steyaert S, Ahmed FM, Harris IR, Teillet J (1997) Characterisation of high temperature oxidation of Nd–Fe–B magnets. J Magn Magn Mater 173:29–42
4. Li Y, Evans HE, Harris IR, Jones IP (2003) The oxidation of NdFeB magnets. Oxid Met 59:167–182
5. Schüler D, Buchert M, Liu R, Dittrich S, Merz C (2011) Study on rare earths and their recycling. Oeko-Institut e.V, Darmstadt
6. Koen B, Peter TJ, Bart B, Tom VG, Yongxiang Y, Allan W, Matthias B (2013) Recycling of rare earths: a critical review. J Clean Prod 51:1–22
7. Nan J, Han D, Yang M, Cui M, Hou X (2006) Recovery of metal values from a mixture of spent lithium-ion batteries and nickel-metal hydride batteries. Hydrometallurgy 84:75–80
8. Saito T, Sato H, Ozawa S, Yu J, Motegi T (2003) The extraction of Nd from waste NdFeB alloys by the glass slag method. J Alloy Compd 353:189–193
9. Uda T (2002) Recovery of rare earths from magnet sludge by $FeCl_2$. Mater Trans 43:55–62
10. Takeda O, Okabe TH, Umetsu Y (2006) Recovery of neodymium from a mixture of magnet scrap and other scrap. J Alloy Compd 408–412:387–390
11. Takeda O, Okabe TH, Umetsu Y (2004) Phase equilibrium of the system Ag–Fe–Nd, and Nd extraction from magnet scraps using molten silver. J Alloy Compd 379:305–313
12. Tang K, Ciftja A, Wilson S, Tranell G (2013) Recycling of the rare earth oxides from spent rechargeable batteries using waste metallurgical slags. J Min Metall Sect B 49(2):233–236
13. Martinez AM, Kjos O, Skybakmoen E, Solheim A, Haarberg GM (2012) Extraction of rare earth metals from Nd-based scrap by electrolysis from molten slag. ECS Trans 50:453–461
14. Miura K, Itoh M, Machida K-I (2008) Extraction and recovery characteristics of Fe element from Nd–Fe–B sintered magnet powder scrap by carbonylation. J Alloy Compd 466:228–232
15. Keene BJ et al (1995) Slag atlas, 2nd edn. Verlag Stahleisen, Düsseldorf
16. Adachi G-Y, Imanaka N (1998) The binary rare earth oxides. Chem Rev 98:1479–1514
17. Zinkevich M (2007) Thermodynamics of rare earth sesquioxides. Prog Mater Sci 52:597–647
18. Sepehri-Amin H, Ohkubo T, Shima T, Hono K (2012) Grain boundary and interface chemistry of an Nd–Fe–B-based sintered magnet. Acta Mater 60:819–830
19. Hallemans B, Wollants P, Roos JR (1995) Thermodynamic assessment of the Fe–Nd–B phase diagram. J Phase Equilib 16:137–149
20. Van Ende MA, Jung IH (2013) Critical thermodynamic evaluation and optimization of the Fe–B, Fe–Nd, B–Nd and Nd–Fe–B systems. J Alloy Compd 548:133–154
21. Hamano H, Kuroda Y, Yoshikawa Y, Nagao M (2000) Adsorption of water on Nd2O3: Protecting a Nd2O3 sample from hydration through surface fluoridation. Langmuir 16:6961–6967
22. Ji Y, Liang J, Chen Z, Xie S (1991) Phase relations in the system $Al_2O_3–B_2O_3–Nd_2O_3$. J Am Ceram Soc 74:444–446
23. Goller G, Toy C, Tekin A, Gupta CK (1996) The production of boron carbide by carbothermic reduction. High Temp Mater Process (London) 15(1–2):117–122
24. Key TS, Crist B (2005) Metastable states in alumina-rich La_2O_3:Al_2O_3 and Nd_2O_3:Al_2O_3. J Am Ceram Soc 88(1):191–195
25. Miki T, Tsujita K, Ban-ya S, Hino M (2006) Activity measurement of the constituents in molten Fe–B and Fe–B–C alloys. CALPHAD 30:449–454
26. Keene BJ (1988) Review of data for the surface tension of iron and its binary alloys. Int Mater Rev 33:1–37